

NEW FEATURES OF UNGUIDED BODY REENTRY WITH SUBCIRCULAR VELOCITY AND PECULIARITIES OF ITS SIMULATION

A.S. Filatyev and A.A. Golikov
Central Aerohydrodynamic Institute (TsAGI)

Keywords: *dispersion area separated part, unguided reentry.*

Abstract

New features of unguided body reentry with subcircular velocity are exposed.

It is demonstrated that trajectories of unguided body are generally unstable because of quasistabilization of angular oscillations on the final flight segment, where the body moves with rather low velocity. Due to the instability the set of ground impact points gains the structure that is qualitative different from the traditional "dispersion ellipse".

The theoretical results are confirmed by numerous outcomes of computer simulation of reentry of separated parts of space launchers and its fragments.

1 Introduction

Investigation of dispersion of unguided body trajectories in the atmosphere has a long-standing background from the origin of artillery. New interest to the problem has been aroused in connection with creation of space launchers (SL). Expanded structure elements of multistage SL are dropped during ascent to increase the payload.

Separated parts (SP) of SL and SP fragments, which can appear in case of SP destruction in dense atmospheric layers, perform unguided reentry until ground impact. The fallout is environmental contamination and probable property damage, health and life threats if the

ground impact points (GIPs) are outside the given alienation zone (AZ).

The practical estimation of possible SP impact areas is traditionally held considering a nominal trajectory that is calculated at ideal conditions of deterministic motion and small deviations under the influence of random factors [1]. The nominal trajectory is assumed ballistic with negligible aerodynamic lift. This hypothesis is based on the supposition of a fast SP angular oscillations in dense atmospheric layers with zero period-averaged lift [2], [3].

However, in frames of the mentioned hypothesis it is difficult to explain extended deviations of some GIPs from the nominal, predicted by the ballistic analysis, at real launches. Such incidents do not occur so infrequently that it may be unlikely to explain by the Gaussian distribution.

According to [4] in general case the non-simply connected *nominal set of GIPs* (NSGIP) appears instead of alone nominal point established traditionally by the ballistic approach mentioned above and accepted in practice. The NSGIP has a ring-type shape (Fig. 1) with the diameter that can exceed reference dimensions of the AZ.

The physical cause of the mentioned phenomenon is the trajectory instability owing to body quasistabilization at the trim angle of attack with nonzero lift and virtually random bank angle at the pre-impact trajectory segment with a low speed.

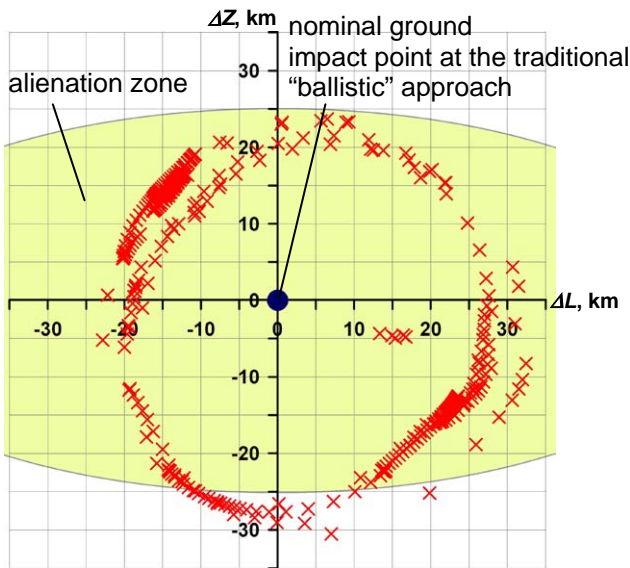


Fig. 1. Revealed qualitatively new topology (ring-type) of a nominal set of ground impact points [4].

The dispersion area can increase in the case of body destruction due to aerothermodynamic loads.

Investigation of the qualitative phenomena needs detailed simulation of full spatial motion, taking into account aerodynamic forces and torques and attitude dynamics as well as influence of random factors.

2 Simulation of body spatial motion

The unguided body spatial motion was calculated on the 6D-differential equation set using the direction cosine matrix with the optimal correction by normalization conditions [5] to avoid singularities.

The investigations of unguided body motion peculiarities include the analysis of influence of initial conditions and body parameters, which led to the qualitative reconstruction of NSGIP, and influence of random perturbation factors on body reentry trajectories and GIP dispersion. These factors embrace body characteristics and atmospheric parameters including wind. Peculiarities of reentry trajectories of SP of SL and its fragments after destruction were also fulfilled.

For the methodical purpose the calculations were carried out for an axisymmetric cylindrical body with a conic dulled nose and a nozzle at aft (Fig. 2). This layout is a typical for common

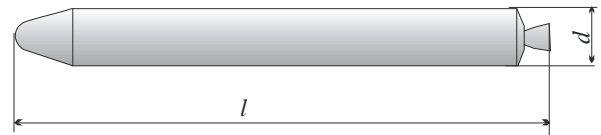


Fig. 2. Aerodynamic layout of the typical booster.

boosters of Delta IV, Atlas V, and Angara. Characteristics of the booster are presented in Table 1.

Table 1. Booster characteristics.

№	Characteristic	Value
1	Diameter-to-length ratio d/l	10
2	Nozzle relative length	0.06
3	Cone angle, degrees	20
4	Ratio of nose radius to body diameter	0.25
5	Moments of inertia (related to the mass and squared length)	$I_x = 1.5 \cdot 10^{-3}$, $I_y = I_z = 6.5 \cdot 10^{-2}$, $I_{xy} = -8 \cdot 10^{-5}$, $I_{xz} = 6 \cdot 10^{-4}$, $I_{yz} = -1.5 \cdot 10^{-5}$.
6	The specific load on the longitudinal section, N/m^2	1400

The booster-type body has a several trim angles of attack α . The typical dependence of aerodynamic pitching moment coefficient C_m on α in the range of $(-180^\circ, 180^\circ]$ has two stable (α_1 and α_{-1}) and two unstable (α_0 and α_2) equilibrium points. The angle α is counted off longitudinal axis towards to the nozzle (Fig. 3).

The aerodynamic damping is not considered to accent the angular stabilization effect due to the energy dissipation at an atmospheric descent.

The reference time of trajectory and attitude motion differs in orders. Therefore it is important to control an accuracy of computer simulation. For this purpose the analytical evaluation and numerical Runge method [7] are used.

Two considered variants of initial conditions are presented in Table 2: the altitude h , velocity V , path angle γ , dynamic pressure q and unit vector \mathbf{e}_ω of the angular velocity (the modulus of angular velocity is $\omega_0 = 1.08$ deg/s).

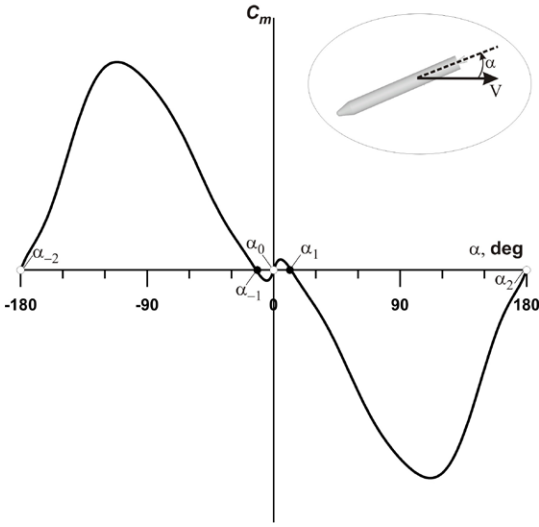


Fig. 3. Dependency of aerodynamic pitching moment C_m on the angle of attack α .

Table 2. Initial conditions.

#	h , km	V , km/s	q , $\text{N}\cdot\text{m}^{-2}$	γ , $^\circ$	\mathbf{e}_ω
1	40	1.7	6000	23	(-0.54, 0.65, -0.54)
2	90	3.0	40	14	(-0.42, 0.68, -0.60)

The initial conditions #2 correspond to SL separation in less dense atmospheric layers than #1.

Let us firstly consider the features of spatial body motion without random factors and destructions. Peculiarities of unguided reentry with subcircular velocities are theoretically studied in [2], [3], [6]. In particular, conditions of the rotary-to-oscillatory motion transition in the atmosphere, so called ‘‘aerocapture’’, and the effect of reducing the oscillation amplitude A with growth of the dynamic pressure q were determined:

$$A \sim q^{-1/4}. \quad (1)$$

In [8], [9] the analytical solution for state and conjugate sets of equations and the qualitative analysis of a nonequilibrium reentry with velocities less than the circular one V_{circ} was established on the base of the asymptotic expansion matching. The existence of the critical initial velocity V_{crit} at which the dynamic pressure and loads on the reentry trajectory are reached the maximum:

$$V_{crit} \leq \frac{V_{circ}}{\sqrt{2}}, \quad (2)$$

was proven. The maximum dynamic pressure at the critical initial velocity can exceed ones on reentry trajectories with higher, near-circular velocities in many times or even in orders.

Let us consider the attitude motion in the plane (Fig. 4), which is normal to the current velocity vector, and watch over projection of the body tail point (nozzle) on this plane, i.e. the hodograph of the point K . The origin point O corresponds to the body mass center and projection of the velocity vector. The length of segment OK' is proportional to $\sin \alpha$. Level lines of equal α are circles. The angle between segment OK' and the plane that contains the local vertical and velocity vector is the spatial bank angle $\sigma \in [-\pi, +\pi]$.

If the booster was separated at relatively high dynamic pressure (variant #1), then an intensive rotation begins around the center of mass because of aerodynamic instability, large aerodynamic moments and the tendency of the amplitude growth according to (1). The ‘‘aerocapture’’ does not happen, i.e. the rotation does not pass into an oscillation with limited amplitude down to ground impact. This causes averaging the aerodynamic lift to zero, so the fall trajectory is near to the ballistic one in accordance with the traditional hypothesis usually used at the ballistic analysis. The typical hodograph of the tail point K under initial conditions #1 is shown in Fig. 5.

At the initial conditions #2 three principal flight segments can be distinguished (Fig. 6). In

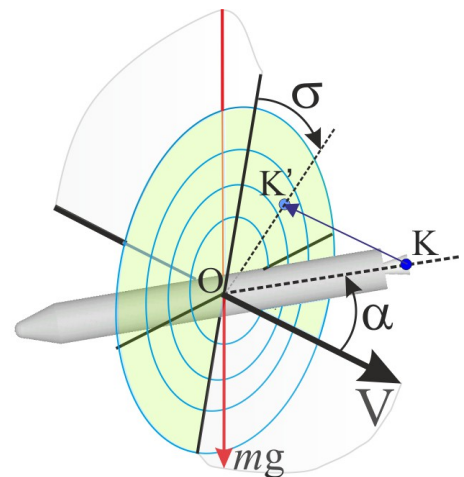


Fig. 4. The scheme of definition of the spatial angle of attack α and bank angle σ .

the beginning, body flight is going at small dynamic pressure and aerodynamic loads. The trajectory is close to Keplerian one and the body rotates owing to separation conditions.

As far as the dynamic pressure grows after entry into dense atmospheric layers, the initial body rotation turns to short-period oscillations (“aerocapture”) at the vicinity of the zero angle of attack, since aerodynamically stable angles of attack at hypersonic segment are rather small (Fig. 3). Reduction in the oscillation amplitude is defined according to (1). At the maximum dynamic pressure the amplitude becomes minimal.

At the final pre-impact flight segment with low velocities, the dynamic pressure and loads are moderate. The quasistabilization at a trim angle of attack with nonzero lift takes place while a bank angle drifts slowly (the body is aerodynamically neutral by the bank angle).

The typical hodograph of the tail point K for the initial conditions #2 is shown in Fig. 7. Here, the quasistabilized bank angles σ are small and the body glides down ensuring almost the maximum longitudinal range.

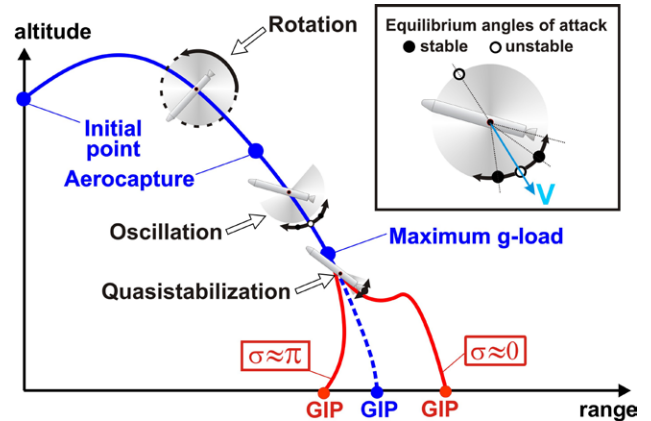


Fig. 6. The trajectory scheme of unguided reentry at the initial conditions #2.

3 Nominal set of ground impact points

Thus, the ballistic approach to definition of the nominal trajectory of unguided body without taking into account a lift due to its averaging to zero is not valid in a general case.

As the bank angle on the quasistabilization segment after passing the maximum dynamic pressure section possesses practically random

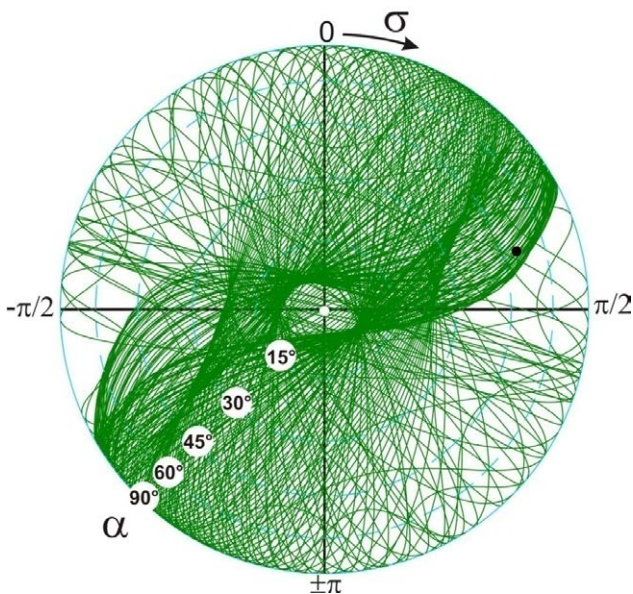


Fig. 5. The hodograph of the booster tail point at reentry with the initial conditions #1,
 ○ – the initial point,
 ● – the ground impact point.

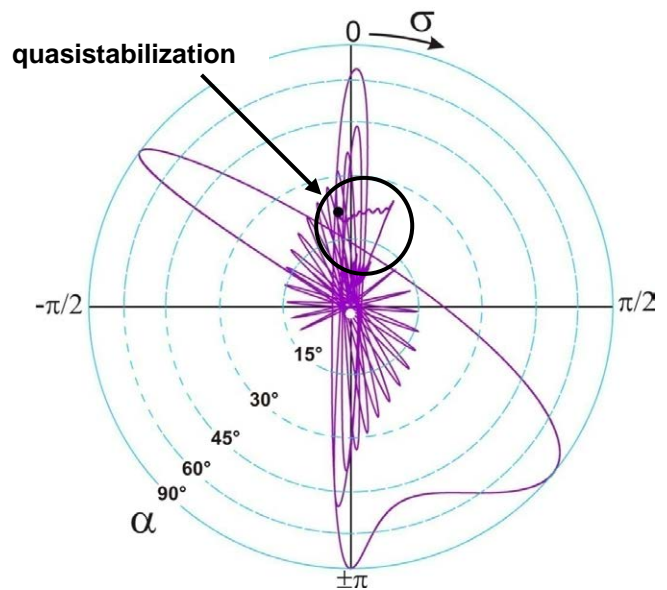


Fig. 7. The hodograph of the booster tail point at reentry with the initial conditions #2,
 ○ – the initial point,
 ● – the ground impact point.

value, the lift orientation is arbitrary. The longitudinal and lateral range deviations of a GIP grow as the trim lift-to-drag ratio becomes greater.

Thus, the nominal trajectories generate a continuum set in the form of a trajectory flow (Fig. 8). Even at absence of random disturbances it is necessary to expect a quasi-circular dispersion of GIPs owing to a described phenomenon. Generally, we have to consider not a single nominal GIP relevant to a ballistic trajectory with average aerodynamic drag distribution, but a nominal set of ground impact points (NSGIP).

For a numerical generation of NSGIP it is enough small disturbances, for example of the initial angular velocity ω_0 , as the relation of GIP coordinates to ω_0 has a character of a white noise [10].

Figure 9 presents NSGIP from 400 GIPs on the plane of longitudinal ΔL and lateral ΔZ displacements and hodographs of the booster tail point after passing maximum dynamic pressure for four values of ω_0 , which correspond approx-

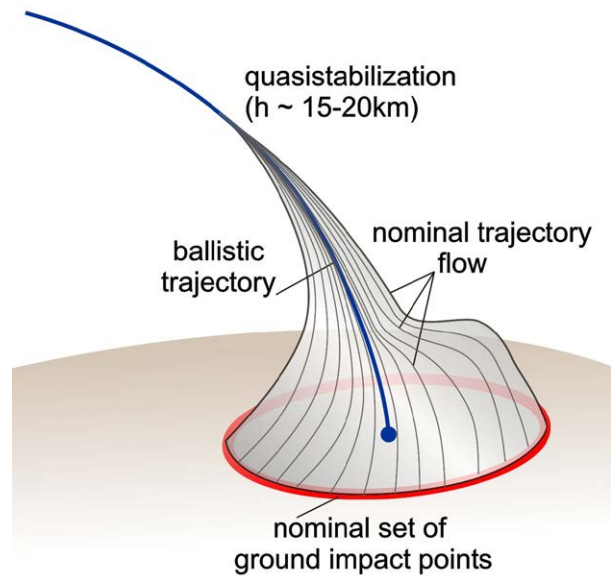


Fig. 8. The nominal trajectory flow induced by the aerodynamic quasistabilization with a nonzero lift.

imately to the maximum and minimum booster longitude ranges and the maximum booster lateral ranges to the right and left sides. Up to achievement of the maximum dynamic pressure the trajectories practically coincide. The dispersion of GIPs on the plane (ΔL , ΔZ) is caused by

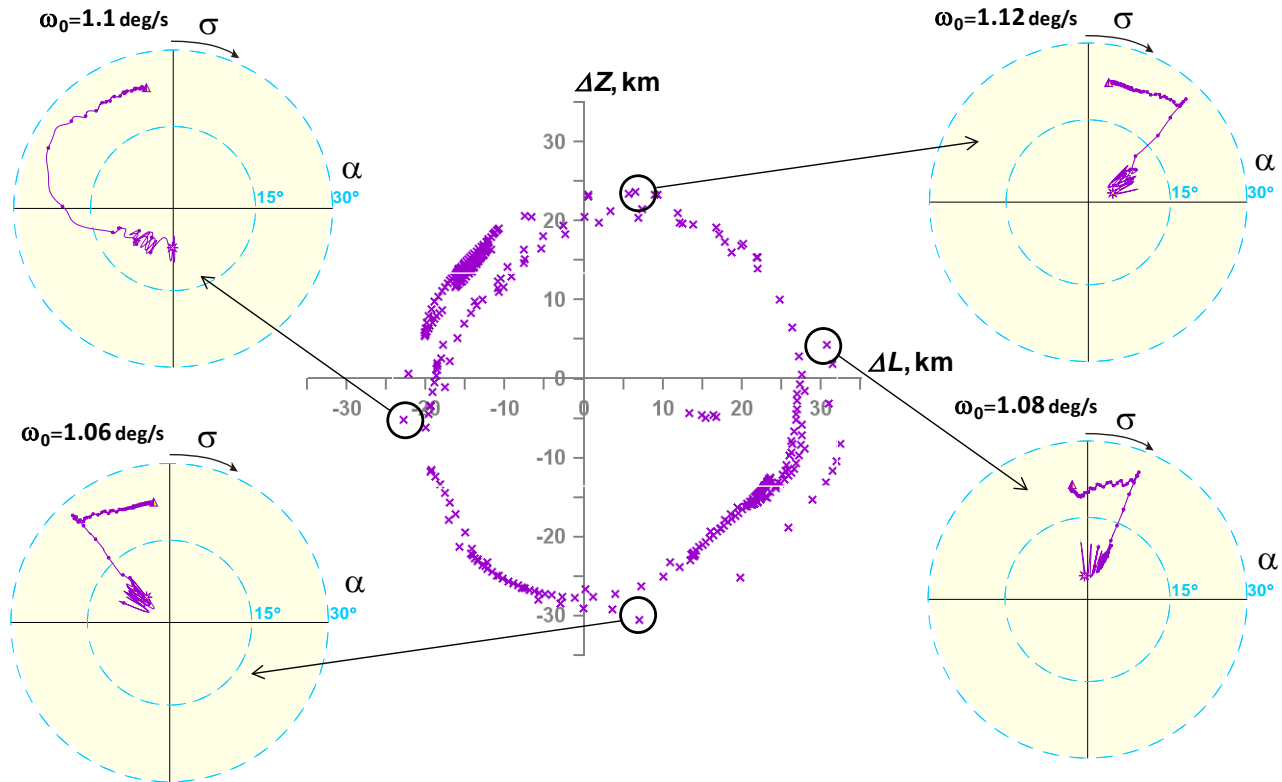


Fig. 9. Nominal set of ground impact points on the plane (ΔL , ΔZ). For four points the hodographs of the body tail point after passing maximum dynamic pressure are shown (in hodographs: \oplus – instant of maximum dynamic pressure, \triangle – impact point).

a variation of ω_0 from 0.92 deg/s to 1.32 deg/s with the step of 0.001 deg/s. This step is essentially less (in five orders) than a reference body angular velocity in dense atmospheric layers (variant #1).

Depending on the steady bank angle after quasistabilization it is reached the maximum (at $\omega_0=1.08$ deg/s) or the minimum (at $\omega_0=1.10$ deg/s) longitudinal range, the maximum lateral range to the left (at $\omega_0=1.12$ deg/s) or to the right (at $\omega_0=1.06$ deg/s).

In considered case the reference size of NSGIP is about 60 km, i.e. it virtually exhausts the intended GIP dispersion areas of current space launchers even without taking random disturbances into consideration.

As mentioned above, the qualitative change of the shape and reference size of the NSGIP due to initial conditions variation is caused by the presence or absence of body aerocapture during a reentry in dense atmospheric layers. Due to the discrete nature of this phenomenon, the qualitative change of the NSGIP appears with a jump [10].

Shown in Fig. 10 is the example of the dependency of the NSGIP reference size D on initial angular velocity ω :

$$D(\omega) = \max_{i,j} \sqrt{(Z_i - Z_j)^2 + (L_i - L_j)^2},$$

where L_i and Z_i are the longitudinal and lateral range of i -th ground impact point at initial pitch angle ν_i , $L_i = L(\nu_i, \omega)$, $Z_i = Z(\nu_i, \omega)$.

It can be seen, that the critical value $\omega_{bif} \approx 2.6$ deg/s of the initial angular velocity exists. If $\omega_0 < \omega_{bif}$, the ‘‘aerocapture’’ of the body in dense atmospheric layers appears that leads to the quasistabilization of the angle of attack at the stable equilibrium value. As a result, the NSGIP ‘‘explodes’’ with its reference size increasing in orders, here from ~ 1 km to ~ 20 km and more.

4 Effect of random disturbances and body fragmentation

The shape of a dispersion area is determined by the aggregate effect of several factors. At absence of the random disturbances causing the

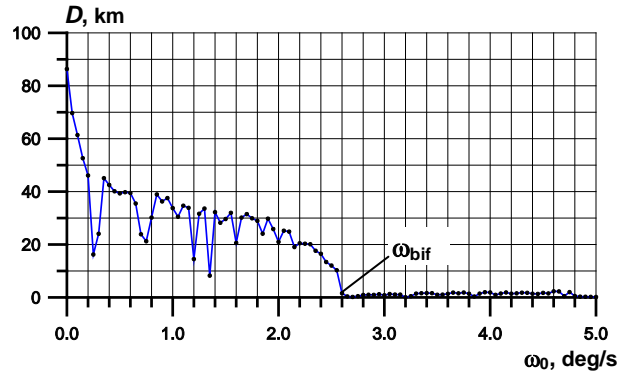


Fig. 10. The NSGIP reference size versus the initial angular velocity ω_0 .

considerable scattering of ground impact points, instability of a trajectory is the dominated factor and the dispersion area has the shape of a ring (Fig. 9). At an operation of the strong random disturbances the area gains a shape of ellipse. Changes in dispersion areas of ground impact points while changing in ratio between scattering induced by random disturbances and instability of trajectory are shown in Fig. 11.

Figure 12 shows the estimation of a dispersion area owing to instability of trajectory and atmospheric disturbances determined on the basis of [11]. At initial conditions #2 it has the nonsimply connected shape with reference size ~ 90 km. If other types of disturbances such as uncertainty of body aerodynamic characteristics, a position of mass center etc. were taken into account the dispersion area can grow even greater.

The main practical conclusion of investigations of a spatial body motion is the fact that reduction in random disturbances cannot cardinaly reduce the size of dispersion area below a

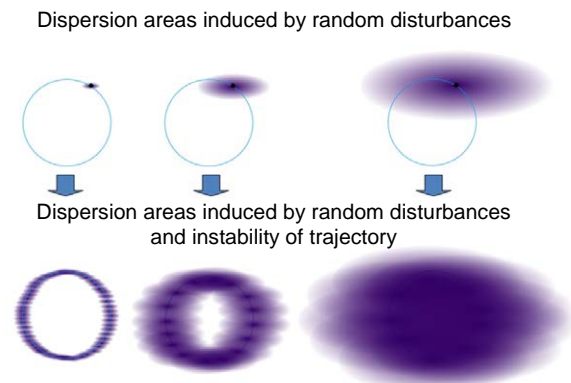


Fig. 11. Changes in dispersion areas of ground impact points while changing in ratio between scattering induced by random disturbances and instability of trajectory.

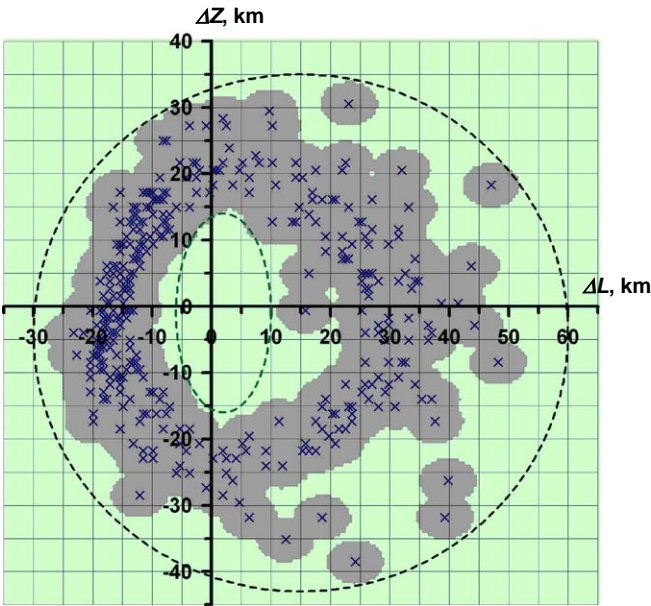


Fig. 12. The estimation of a dispersion area owing to instability of trajectory and atmospheric disturbances.

marginal level, which is defined by instability of trajectories (about 40 km).

On phases of a non-equilibrium body reentry into an atmosphere with subcircular velocities the peak aerothermodynamic loads can surpass in orders a level realized at a pseudo-steady drop with near-circular velocities [8],[9]. Extreme loads can result in destruction of the body. After primary destruction, as a rule, there is the further destructions of body fragments. By virtue of the fact that the aggregate heat flows are insufficient for complete combustion of fragments which can have high aerodynamic carrying properties, the dispersion area will sharply increase that is undesirable because of ecological repercussions, especially for perspective space launchers.

For typical SL booster, which consists of tanks, interstages and engines, the estimations of the destruction moments were obtained based on the analysis of stress-strain state of a structure in view of an intrinsic pressure by a technique explained in [12]. In accordance with preliminary outcomes of simulation, the body destruction at atmospheric reentry is most probably the result of strength degradation of materials owing to heating. Destruction has character of explosion, thus the prediction of particular characteristics of fragments without the analysis of flight experiment becomes difficult.

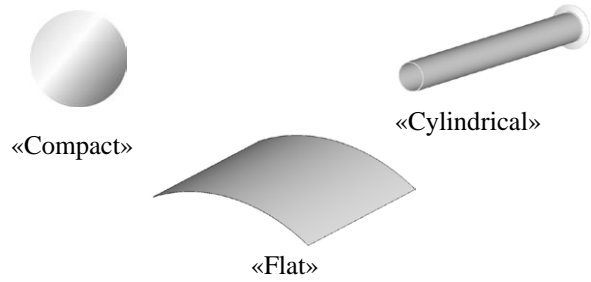


Fig. 13. Referenced layouts of 3 fragment types.

Separate dispersion researches of 3 various fragment types are of interest:

A. Fragments of the “compact” shape which reference sizes on three axes are approximately equal.

B. Fragments of the “flat” shape which reference size on one of axes are much less than size on two other axes.

C. Fragments of the “cylindrical” shape which reference size on one of axes are much greater the size on two other axes.

For each type of fragments the reference layout (Fig. 13) and the corresponding aerodynamic characteristics were determined:

A. The reference layout of “compact” fragments was an orb. The aerodynamic drag coefficient C_D was set equal to the drag coefficient of an orb at Reynold's number $Re=10^6$ with the lift being equal to zero.

B. The reference layout of “flat” fragments was a lateral surface of the cylinder with a sector angle of 60° (Fig. 13). Average thickness δ and density of material ρ were supposed to be defined. Then fragments of the miscellaneous sizes are dynamically similar in terms of forces, for example, a ballistic coefficient

$$\frac{C_D S_{ref}}{m} = \frac{C_D \cdot l \cdot 0.5d}{\rho \delta l \cdot \frac{\pi}{3} \cdot 0.5d} = \frac{3C_D}{\pi \rho \delta} \quad (3)$$

does not depend neither on length l , nor on diameter of cylinder d . In (3) and below, m is the mass of the fragment, S_{ref} is the reference area. A unit load on the cross-sectional area

$$\frac{m}{S_{ref}} = \frac{\pi \rho \delta}{3}$$

is constant and supposed to be equal to 4600 N/m^2 .

B. The reference layout of “cylindrical” fragments was a flange pipe (Fig. 13). Wall thickness δ , density of material ρ and length-to-diameter ratio were supposed to be defined,

$$\frac{l}{d} = 9. \quad (4)$$

Fragments with different length are similar in terms of forces. For example, the ballistic coefficient remains constant:

$$\frac{C_D S_{ref}}{m} = \frac{C_D \cdot \pi d^2}{\rho \pi d \delta l} = \frac{C_D d}{\rho \delta l}.$$

A unit load on the cross-sectional area

$$\frac{m}{S_{ref}} = \frac{\rho \delta l}{d}$$

is constant and supposed to be equal to 4600 N/m².

To estimate the dispersion areas of body fragments under operation of large number of random factors the technique based on following assumptions was used:

1. The moment of body fragmentation was supposed random and the distributed under the normal law on time. Root-mean-square deviation σ was set so that 3σ corresponds to a difference in time between a maximum of a density function and a maximum of a heat flow on a glide trajectory of a non-destructed body.

2. Initial coordinates and angular velocity of fragments coincide with the similar values of the body at the moment of destruction. The linear velocity of fragments is supposed to take additional increment with regard to velocity of the body. The increment is randomly directed and has random value with uniform distribution in the range from 0 to 200 m/s.

3. For each of 3 types of fragments the random parameter with a uniform distribution which describes some set of fragments of the given type was assigned.

A. The ballistic coefficient is defined as random parameter of “compact” fragments. The simulation of gliding is conducted separately for “light” fragments (a ballistic coefficient from $6 \cdot 10^{-4}$ to $6 \cdot 10^{-3}$) and “heavy” fragments (a ballistic coefficient from $2 \cdot 10^{-4}$ to $2 \cdot 10^{-3}$).

B-C. Random parameter of “flat” and “cylindrical” fragments is the length l . For frag-

ments of the “flat” shape it was set in the range $1.0m \leq l \leq 4.0m$, for fragments of the “flat” shape it was in the range $0.9m \leq l \leq 2.7m$.

When fragment trajectories of “cylindrical” and “flat” type statistically simulating the random fluctuations of characteristics with a uniform distribution were set additionally (Table 3).

Table 3. The maximum deviations of characteristics from defined values

Characteristics	Maximal specific deviation	
	“cylindrical”	“flat”
Aerodynamic force coefficients	±15%	±30%
Aerodynamic moment coefficients	±5% (center of pressure)	±30% (rolling, pitching and yawing moments)
Fragment density	±10%	±10%
Mass center position	±1%	±1%

The selected approach allows conducting the statistical simulation of fragment trajectories with the use of aerodynamic characteristics for reference layouts only to reduce essentially the calculation time.

Figure 14 presents the results of the dispersion area estimation based on simulation of 2000 trajectories of every fragment type. The initial conditions of the body correspond to variant #2.

By results of a statistical analysis the following conclusions can be made:

1. Ground impact points of “compact” fragments, which are similar to an orb, have the greatest longitudinal range and the least lateral dispersion.

2. The greatest lateral dispersion is observed for “flat” fragments having high aerodynamic carrying properties (a root-mean-square deviation is approximately in 1.5 times more than for fragments “compact” types). It is possible to explain the given effect by a stabilization of fragment rotation around the mass center at particular combination of aerodynamic characteristics and the prolonged motion with high lift-to-drag ratio.

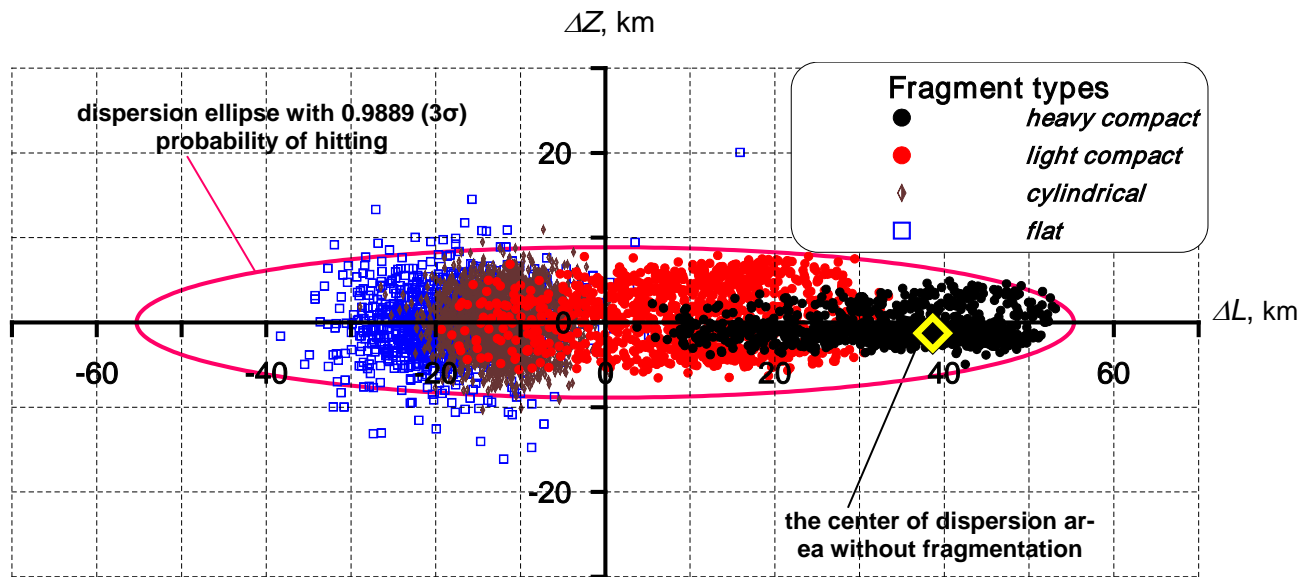


Fig. 14. Dispersion areas of ground impact points for four fragment types.

Conclusions

Trajectories of unguided body reentry with subcircular velocities are generally unstable because of quasistabilization with a nonzero lift at a pre-impact segment with a relatively low speed. The trajectory instability manifests itself as an additional and often dominant random factor.

As a result, in the general case the dispersion area of ground impact points differs essentially from the traditional “dispersion ellipse”. In these cases the maximum probability density can be dispersed quasi-uniformly over a circle-type line. The radius of the circle can exceed in orders the dimension of the traditional dispersion ellipse even for customary aerodynamic layouts.

An increase of the staging velocity and altitude of a space launcher can lead to the “explosive” (bifurcational) expansion of the dispersion area of ground impact points in orders.

References

- [1] Appazov R.Ph., Sytin O.G. *Methods of designing launchers and spacecraft*. Moscow, “Nauka”, 1987 (in Russian).
- [2] Kuzmak G.E. *Dynamics of unguided motion of aircraft at an atmospheric reentry*. Moscow, “Nauka”, 1970 (in Russian).
- [3] Yaroshevsky V.A. *The motion of an unguided body into the atmosphere*. Moscow, “Mashinostroyeniye”, 1978 (in Russian).
- [4] Golikov A.A., Demeshkina V.V., Leutin A.P., Filat'ev A.S. Peculiarities of unguided reentry of space transportation system parts, *Doklady Physics*, Vol. 55, No.12, 2010, pp. 597 - 601.
- [5] Shilov A.A. The optimal correction of the direction cosine matrix in rigid body motion calculations. *Uchenye zapiski TsAGI*, 1977. No. 5 (in Russian).
- [6] A. Busemann, N.X. Vinh and R.D. Culp. *Hypersonic and Planetary Entry Flight Mechanics*. The University of Michigan Press, Ann Arbor, 1980.
- [7] E. Hairer, S.P. Norsett, G. Wanner. *Solving Ordinary Differential Equations I. Nonstiff Problems*. Springer-Verlag Berlin Heidelberg, 1987.
- [8] Filatyev A.S. The approximate analytical synthesis of the hypersonic aircraft optimal control in an atmospheric motion with a subcircular velocity, parts 1, and 2. *Uchenye zapiski TsAGI*, vol. XI, Nos. 1, 2, 1980 (in Russian).
- [9] Filatyev A.S. «Paradoxes» of optimal solutions in problems of space vehicle injection and reentry. *Acta Astronautica*, vol. 47, issue 1, 2000.
- [10] A.S. Filatyev, A.A. Golikov, V.V. Demeshkina, M.E. Karasev, A.P. Leutin. Peculiarities of computer simulation of unguided reentry of space transportation system parts. *Proceedings of the 61st International Astronautical Congress*, Prague, Czech republic, 27 September - 1 October 2010, Paper IAC-10.D2.3.12.

- [11] Filatyev, A.S., and Yanova, O.V. Through optimization of branching injection trajectories by the Pontryagin maximum principle using stochastic models. *Acta Astronautica*, vol. 68, Issues 7-8, pp. 1042-1050, April-May 2011.
- [12] Dubovikov E.A. Method and Software Algorithm of Simulating the Inner and Outer Loading of Carrier Rocket Airframe in Atmosphere on the Basis of Automated Strength Model. “*Nauchnyi vestnik MSTU CA*”, №172, 2011, pp.178-183 (in Russian).

Copyright Statement

The authors confirm that they, and/or their company or organization, hold copyright on all of the original material included in this paper. The authors also confirm that they have obtained permission, from the copyright holder of any third party material included in this paper, to publish it as part of their paper. The authors confirm that they give permission, or have obtained permission from the copyright holder of this paper, for the publication and distribution of this paper as part of the ICAS 2014 proceedings or as individual off-prints from the proceedings.